

Polyoxometalates

Regioselective Catalysis by the {Mo₁₃₂} Nanocapsule:
A Computational InspectionNuno A. G. Bandeira^[a,b,c] and Carles Bo^{*[a,d]}

Abstract: By means of density functional calculations, we perform a mechanistic analysis of the Huisgen cycloaddition reaction taking place with the chemical involvement of the {Mo₁₃₂} nanocapsule, initially reported by Besson and others [*Dalton Trans.* **2012**, *41*, 9852–9854], whereby a 2:1 regioselectivity is obtained by chemically grafting the reactants onto the cavity walls of this metal-oxide catalyst. We explore the mechanistic pathways quantitatively and explore the basis of this regioselectivity.

When propiolate is coordinated to the nanocapsule, the selectivity of the catalytic system is both kinetically and thermodynamically in favour of the formation of 1,4-triazole, whereas in the alternative pathway, which begins with the triazidoacetate coordination, the selectivity is kinetic alone. The former and latter pathways have activation barrier differences between each isomer of 29.9 kJ/mol and 39.2 kJ/mol, respectively.

Introduction

Polyoxometalates^[1] are a class of materials that have gained a variety of uses^[2] over the years, chiefly among them being their use in catalysis,^[3] due to their highly acidic properties. Of notable interest is the molybdenum Keplerate nanosphere^[4] (Figure 1), formulated as $\{[(\text{Mo}^{\text{VI}}(\text{Mo}^{\text{VI}}_5\text{O}_{21})(\text{H}_2\text{O})_6)_{12}(\text{Mo}^{\text{V}}_2\text{O}_4(\text{L}^{n-}))_{30}]^{(12+30n)-}$ (hereafter {Mo₁₃₂}) which is a significant breakthrough in the field, since due to its porous molecular structure, it allows the confinement of small molecules in a spherical molecular container akin to the Bucky ball, but with very different properties, since the metal–oxo bonds are very polar.

This {Mo₁₃₂} Keplerate therefore has the potential to become a size- and chemically selective nanoreactor.^[5] The first electronic structure study was presented by one of us^[6] and shortly thereafter, came the first detailed experimental and computational study of the catalytic behaviour of this polyanion.^[7] The most commonly used Lⁿ⁻ type of bridging ligands anchored to the {Mo₂O₄} moieties, especially in catalysis,^[7,8] are the carboxylate ligands (formate, acetate, etc.), since they are conveniently labile.

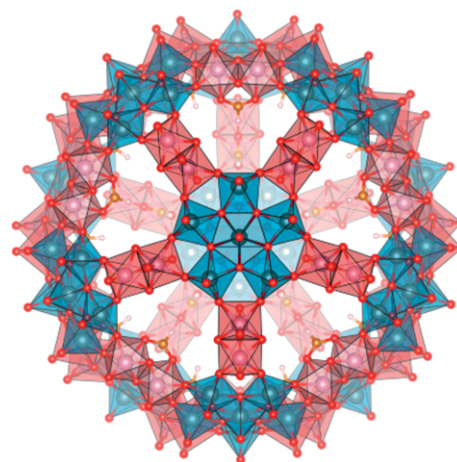


Figure 1. {Mo₁₃₂} structure with interior formate bridging ligands coordinated to the catalytically active {Mo₂O₄} units (in red).

A recent paper by Besson and others^[9] reports a regioselective Huisgen^[10] [$\pi 4_s + \pi 2_s$] cycloaddition reaction within the polynuclear Keplerate anionic $\{[(\text{Mo}^{\text{VI}})\text{Mo}^{\text{VI}}_5\text{O}_{21}(\text{H}_2\text{O})_6]_{12}(\text{Mo}^{\text{V}}_2\text{O}_4(\mu^2\text{-X}))_{30}\}^{42-}$ (X = bridging monoanion) nanosphere, wherein the 2-azidoacetate (X = N₃CH₂COO⁻) encapsulated complex ($\{(\text{Mo}_{132}\text{-N}_3)\}$) was left to react overnight with excess propiolic acid (HC₂COOH) at room temperature, then yielding the products of cyclisation of the type outlined in Scheme 1. The authors reported that the unencapsulated reaction yields a mixture of isomers in a haphazard 1,4-/1,5-triazole ratio, ranging from 0.8 to 8:1, and that the same reaction when taking place within the Keplerate cavity yields a regioselective ratio of 2:1 in favour of the 1,4 triazole product.^[9] These findings are groundbreaking and they potentially lead the way to other regioselective cyclisation reactions of feedstocks to generate high-value chemicals in an environmentally clean (aqueous) medium.

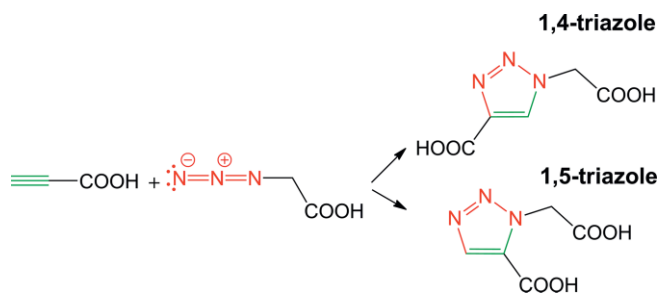
[a] *Institute of Chemical Research of Catalonia (ICIQ), The Barcelona Institute of Science and Technology, Av. dels Països Catalans, 16, 43007 Tarragona, Spain*
E-mail: cbo@icqi.es
http://www.iciq.org/research/research_group/prof-carles-bo/

[b] *BioISI – Biosystems & Integrative Sciences Institute Faculdade de Ciências, Universidade de Lisboa, Campo Grande, 1749-016 Lisboa, Portugal*

[c] *Centro de Química Estrutural, Instituto Superior Técnico, Universidade de Lisboa, Av. Rovisco Pais 1, 1049-001 Lisboa, Portugal*

[d] *Departament de Química Física i Inorgànica, Universitat Rovira i Virgili, Av. dels Països Catalans, 26, 43007 Tarragona, Spain*

Supporting information and ORCID(s) from the author(s) for this article are available on the WWW under <https://doi.org/10.1002/ejic.201800155>.



Scheme 1. Huisgen reaction between carboxylates, yielding a mixture of isomers 1,4- and 1,5-substituted triazoles.

An understanding of the chemical phenomena that take place in this catalytic environment is paramount and an explanation at the molecular level for the underlying reasons of this regioselectivity is warranted. We therefore report, herein, a computational analysis of the reaction pathway of this particular cycloaddition reaction, with and without the presence of a nanoreactor cluster, to attempt to explain its chemical origin.

Results and Discussion

To study the reaction pathway using a model of the whole of the Keplerate sphere, despite its high symmetry, would be computationally intractable; so instead, we chose to employ a reliable and minimal cluster model known to capture the reactivity trends of the Keplerate sphere, as described previously in the literature.^[7,11] The original authors noticed^[9] that upon mixing the reagents, within a few minutes, a mixture of encapsulated azidoacetate/propiolate is detectable by NMR spectroscopy, so that it becomes unclear if the reaction initiates from the azidoacetate or the propiolate chelate. Consequently, both pathways need to be explored.

The working model is the $[(\text{Mo}^{\text{VI}})\text{Mo}^{\text{VI}}_5\text{O}_{13}(\text{H}_2\text{O})_{12}(\text{OH})_8]^{2-}\{\text{Mo}^{\text{V}}_2\text{O}_4(\text{H}_2\text{O})\}^{6+}$ cation $\{\text{Mo}_{14}\}$, which by coordination of either azidoacetate or propiolate to the Mo^{V} centres ($\{\text{Mo}_{14}\text{-N}_3\}$ and $\{\text{Mo}_{14}\text{-C}_2\}$) will have its charge decreased by one unit. The optimised $\text{Mo}^{\text{V}}\text{-O}$ (O-acetate) distances in $\{\text{Mo}_{14}\text{-N}_3\}$ are more contrasting (2.315 and 2.583 Å) than in $\{\text{Mo}_{14}\text{-C}_2\}$ (2.473 and 2.582 Å), likely due to the steric hindrance caused by the azido group, which by engaging in hydrogen bonding with nearby aqua ligands, causes some deformation of the interplanar angle of the star-shaped moieties (Figure 2).

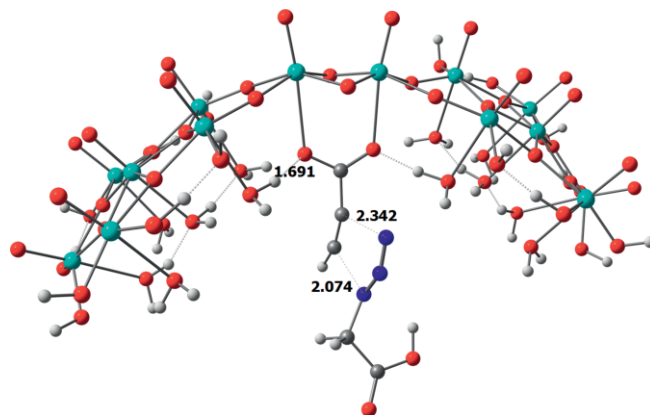


Figure 2. Transition state (TSa), leading to $\{1,4\text{-triazole@Mo}_{14}\}$, with selected bond lengths [Å].

The organic pathway was computed for comparison with the reaction that takes place in the encapsulated environment and will be discussed below. Two main branches will be followed in the mechanistic survey: one beginning with propiolate in anionic or coordinated form (branch **a**) and another with azidoacetate in a like manner (branch **b**).

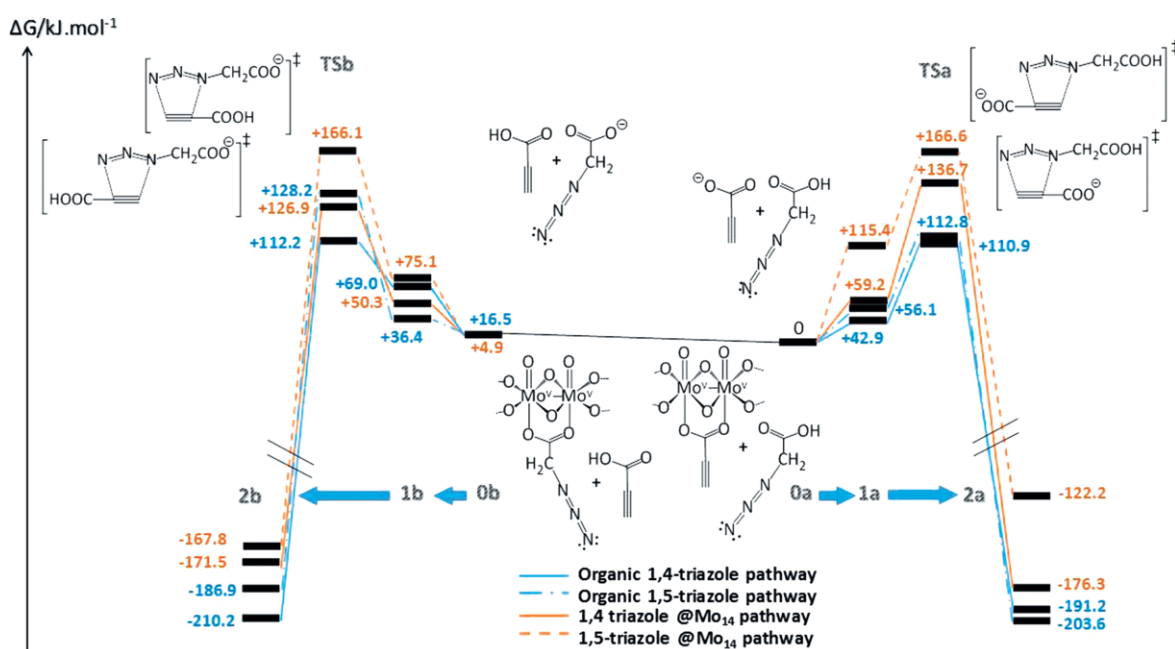


Figure 3. Calculated reaction pathway free energies [kJ/mol] of the coordinated (orange) and uncoordinated (blue) Huisgen reactions.

The Organic Reaction

The energy difference between the {propionate + azidoacetic acid} (**0a**) and the {propionic acid + azidoacetate} (**0b**) systems, where each molecule is infinitely separated from the other, is the proton transfer and this has an energy difference of 16.5 kJ/mol in favour of the {propionate + azidoacetic acid} system (cf. Figure 3).

Pursuing the pathway from **0a** onto the stationary point in which each reactant is assembled (**1a**), we find an endergonic change of +42.9 and +56.1 kJ/mol, respectively, for the molecular pair, resulting in a conformation with neighbouring and remote carboxylate groups. The ensuing transition state (TSa) for both conformations is practically isoenergetic (+110.9 and +112.8 kJ/mol, respectively), but the products (**2a**) are greatly stable and compensate for the energy cost nearly twofold (−191.2 and −203.6 kJ/mol, respectively). We observe that the process is neither kinetically nor thermodynamically selective with regards to a particular product (1,5-triazole or 1,4-triazole) with the chosen solvation model.

Additionally, if we pursue the reaction starting from reactants **0b**, the preassociation of the two molecules **1b** is also endergonic, but their stability is slightly more differentiated in favour of the vicinal (leading to 1,5-triazole) carboxylate groups (with $\Delta G^\circ = +36.4$ versus +69.0 kJ/mol). The two transition states (TSb) are again not too different in energy from each other (± 10 kJ/mol), but eventually, the 1,4-triazole is favoured thermodynamically (−210.2 kJ/mol, with respect to the initial point) vis-à-vis the 1,5-isomer (−186.9 kJ/mol).

Similar barriers were also computed, for the sake of completeness, for the {N₃CH₂COOH + HC₂COOH} and {N₃CH₂COO[−] + HC₂COO[−]} reactants (see the Supporting Information).

The Reaction Inside the Nanocluster

We now turn to the discussion of the cluster-bound molecules. With regards to reaction pathway **a**, where {propionate@Mo₁₄} is the starting reactant, there is a significant difference in energy for the preassociation complexes in the 1,4 conformation position (+59.2 kJ/mol) by comparison with the 1,5 (+115.4 kJ/mol) (**1a**). Thereafter, the transition state of the 1,5-isomer formation has approximately the same hike in free energy as its 1,4 analogue, despite the relative activation barrier being some 30 kJ/mol higher. The final products (**2a**) are differentiated, stability wise, by an order of $\Delta G^\circ = 54$ kJ/mol, again in favour of the 1,4-coordinated isomer.

In pathway **b**, {azidoacetate@Mo₁₄}, the preassociation complexes are not as differentiated in energy (25 kJ/mol) and the ensuing transition-state energies (TSb) are again discriminative of the isomers by a magnitude of 40 kJ/mol.

The coordinated triazole products **2b** are almost isoenergetic, meaning that for the 1,5 isomer to be generated, the **b** pathway is the thermodynamically more favourable choice, although the transition-state barrier for the 1,5-formation is fairly identical in **a** and **b**. The kinetic and thermodynamic unfavourabilities of forming 1,5-triazole through **a** is already

manifested in the electronic energies and are not a consequence of entropy or enthalpic terms. In the **1b** path, this process is balanced out by the added entropy of the 1,5 conformation, which renders it slightly more favourable.

This accounts for the 2:1 isomeric ratio obtained experimentally^[9] for the Keplerate system. The {1,4-triazole@Mo₁₄} system can be formed through both pathways **a** and **b**, whereas the {1,5-triazole@Mo₁₄} is only thermodynamically stable through **b**, with a slower rate of formation than its isomer.

To clarify the physical reasons for the relative barrier heights of the two isomers of the {triazole@Mo₁₄} complex in the **a** pathway, an energy decomposition analysis (see Computational Details) was undertaken on all of the TSa structures, including the organic ones. The selected fragments were the reactant molecules for each reaction and the values are listed in Table 1.

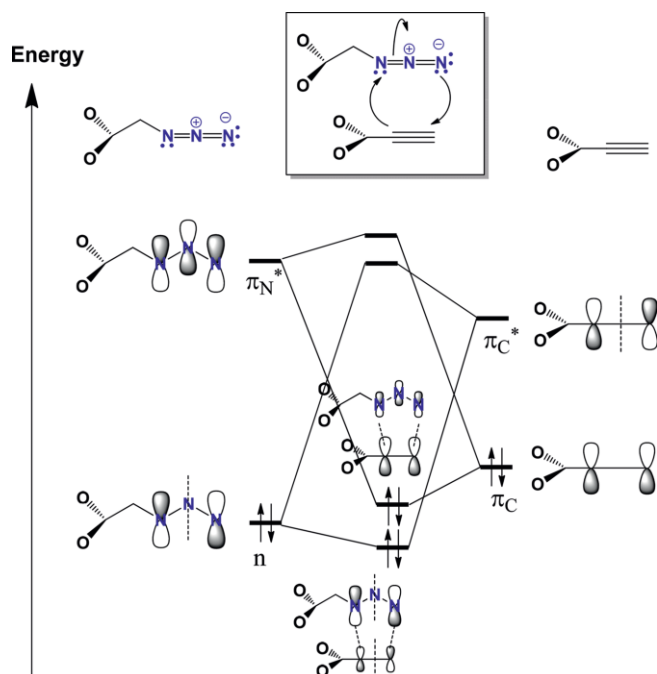
Table 1. Energy decomposition analysis of the TSa transition states.

ΔE	TSa {1,4@Mo ₁₄ } [kJ/mol]	TSa {1,5@Mo ₁₄ } [kJ/mol]	TSa 1,4-triazole [kJ/mol]	TSa 1,5-triazole [kJ/mol]
ΔE_{Pauli}	+362.8	+452.0	+348.8	+360.0
ΔE_{Elect}	−179.9	−217.9	−222.4	−220.9
ΔE_{Orb}	−206.9	−288.3	−180.3	−196.9
ΔE_{Solv}	−3.4	+29.1	+14.2	+17.1
ΔE_{Int}	−27.4	−25.2	−39.7	−40.6
ΔE_{Prep}	+91.0	+121.6	+97.2	+99.2
− D_e	+63.6	+96.4	+57.5	+58.6

While the organic transition states listed on the right-hand side of the table have comparatively identical energy terms and overall interaction energies, the two complexes present significant differences between them. The 1,5-TSa has a much larger Pauli repulsion than the 1,4-TSa, but this is compensated by more favourable electrostatic and orbital interaction energies, while the change in solvation energy has the opposite sign. Nevertheless the interaction energies of both transition states are almost the same (−27 and −25 kJ/mol, respectively). The overall electronic dissociation energy (− D_e), however, favours the 1,4-TSa, due to a lower ligand rearrangement energy (ΔE_{Prep}). It is this latter term that is one of the determining factors in the energy-barrier heights. The other one is the additional Pauli repulsion, not present in the organic transition states, and it can be accounted for by the steric clash between the carboxylate chain and the bridging oxo groups of the {Mo₁₄} cluster.

The molecular orbital interactions present in the bond-formation process are those which are symmetry-allowed in ordinary cycloaddition processes.^[12] From a qualitative frontier molecular orbital description, the nitrogen lone pairs (*n*) in triazidoacetic acid/triazidoacetate are donated to the π_{C}^* orbitals of the propionate/propionic acid, and inversely, the π_{C} orbitals of the latter are donated to the π_{N}^* of the former (Scheme 2). These donor–acceptor interactions are present in the transition states to some degree and they can be quantified by a Mulliken gross population analysis in the basis of the aforementioned fragments (see the Supporting Information).

In all of the transition states, organic and in the cluster complex, these donor–acceptor interactions are relatively small, as



Scheme 2. Simplified MO scheme for the Huisgen cycloaddition reaction with MO composition.

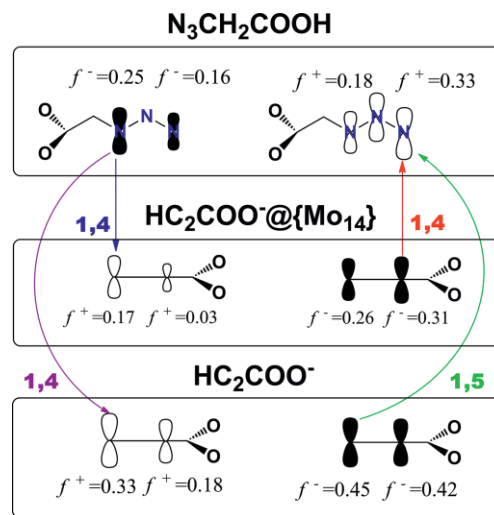
the transition states are significantly unbound. Also, due to polarisation from the relevant fragment molecular orbitals (FMOs) into other MOs, there is a risk of oversimplifying the interaction processes to comply with the frontier MO description.

The HOMO-2 of the 1,4-TSa cluster has a 54 % π_C contribution and a 5 % π_N^* contribution and can be roughly classed as one of the donor-acceptor channels; the HOMO-1 has 92 % n and a rather small 2 % π_C^* (Scheme 2) and is the complementary donor-acceptor channel. The remaining transition-state geometries show a similar electronic behaviour.

If one analyses the isolated reactants in route **a** in terms of descriptors of chemical reactivity, one finds that the regioselectivity exhibited experimentally can be aptly demonstrated by Pearson's HSAB principle.^[13] Inspecting the partial condensed Fukui functions [$f^-(X) \equiv \rho(\pi_X)$, $f^+(X) \equiv \rho(\pi_X^*)$], calculated as the density matrix orbital contributions of the reactive atomic sites of the reactants, we can establish a comparison between the propiolate when it is a free anion and when it is a ligand. When soft nucleophiles and electrophiles react, the attack sites will be the ones with the highest values of the Fukui function, both in the electrophile and the nucleophile.

When propiolate is a free anion, the highest $f^-(N)$ and $f^+(C)$ indices favour the cycloaddition in the 1,4 arrangement, but the remaining $f^-(C)$ indices of both carbon sites (0.45 and 0.42) favour the 1,5 arrangement (Scheme 3). When the propiolate is coordinated to the metal cluster, it undergoes strong polarisation of its electron density, differentiating the atomic sites further, favouring the 1,4 conformational assembly of the reactants in both donor-acceptor channels. The propiolate ligand has its highest $f^-(C)$ index (0.17) in the nonsubstituted acetylenic carbon, thus favouring the nucleophilic attack of the carbon-bonded nitrogen of triazidoacetic acid [$f^-(N) = 0.25$]. The con-

verse electron-density flow is also more favourable in the 1,4 conformation, since this arrangement has the highest $f^-(C)$ and $f^+(N)$ indices.



Scheme 3. Condensed partial nucleophilic and electrophilic Fukui functions for both donor (black)-acceptor (void) channels of coordinated and uncoordinated propiolate with triazidoacetic acid.

The MO occupancies in the FMO basis show the electron outflow from the FMOs and electron intake to the virtual FMOs of the fragments. As a general trend, the electron donation is approximately $0.2 e^-$ to each of the virtual FMOs. It is evident from these values that the donor-acceptor interactions assume equal importance, contradicting the information obtained from the coefficient analysis of the transition states, which privileges the $\pi_C \rightarrow \pi_N^*$ donation.

Conclusion

We performed a comprehensive examination of a regioselective Huisgen reaction mechanism taking place when each reactant is anchored to a $\{Mo_{14}\}$ cluster, as a model of the interior surface of the $\{Mo_{132}\}$ Keplerate. The calculated activation barriers for the formation of the 1,4- and 1,5-triazole isomers differ by 29.9 (a pathway) and 39.2 kJ/mol (b), in favour of the 1,4-triazole, depending on the reactant that is coordinated to the cluster. The $\{propiolate@Mo_{14}\}$ system yields a 1,5-triazole product that is less stable, by +54 kJ/mol, than its isomer and is not the thermodynamically more-viable route for this production. Conversely, the $\{azidoacetate@Mo_{14}\}$ route only discriminates kinetically between the two products.

Steric hindrance, as seen from the Pauli repulsion terms, and a significant fragment distortion energy were shown to be the deciding factors in differentiating the activation barriers.

The regioselectivity of the frontier orbital interactions was examined with respect to the organic reactants and the most favourable donor-acceptor interactions in the $\{propiolate@Mo_{14}\}$ system are the ones that lead to the 1,4-triazole product.

Computational Details

The Amsterdam density functional (ADF) program package,^[14] version 2013.01, was used throughout to optimise the geometries of all species mentioned in the paper. The Becke^[15] and Perdew^[16] gradient-corrected exchange and correlation functionals (BP86), respectively, were used in the calculations. The ZORA^[17] scalar relativistic Hamiltonian was employed with a triple-zeta Slater type orbital^[18] (STO), augmented with one polarisation function (TZP), for molybdenum, and with double-zeta STO type functions, augmented with d functions, for the remaining elements. A small frozen core was used for all elements (1s² shell for O and C; 3d¹⁰ shell for Mo), except hydrogen. The geometry optimisations were performed by using Becke's default numerical integration scheme.^[19] Stationary points were located with normal integration accuracy, whereas partial and full analytic Hessian calculations were done with a "quality = good" integration accuracy and free energies were computed at standard-state conditions. The COSMO^[20] implicit solvation scheme was employed throughout, with the default solute atomic radii. The imaginary frequencies associated with the reaction coordinate were followed by a small fraction of their displacement in either direction, and were subsequently reoptimised to certify the obtainment of the reactant and the product.

The energy decomposition analysis created from Ziegler and Rauk,^[21] based on the initial work by Morokuma^[22] and implemented by others^[23] in ADF, was performed for all TSa transition states, with the default integration grid and the aforementioned solvation method. This fragment-partitioning analysis partitioned the interaction energy ΔE_{Int} into the basis of two or more unrelaxed fragments, with the following terms: ΔE_{Pauli} , ΔE_{Elect} , ΔE_{Orb} and ΔE_{Solv} . ADF yielded the ΔE_{Pauli} and ΔE_{Elect} quantities, which were extracted directly from the output file, since they did not change with the solvation properties. The ΔE_{Pauli} value corresponded to the Pauli repulsion, the difference between the energies of the product of the fragment wavefunction $\Psi_A\Psi_B$ (for fragments A and B) and the energy of its antisymmetrised form $|\Psi_A\Psi_B|_A$, and it was intuitively associated with interfragment repulsion of same-spin electrons. The ΔE_{Elect} term was the quasiclassical coulombic term associated with the frozen charge densities of both fragments in each other's presence, with respect to their infinitely separated state. Two other quantities were considered, ΔE_{Orb} and ΔE_{Solv} which amounted to the energy change in the fragment MO coefficients, due to overlap from bringing the two fragments together, and the energy change due to solvation, respectively. These two terms, with respect to the solvated fragments, were quantities which had to be calculated indirectly through a thermochemical cycle, since ADF only yielded these terms with fragments in vacuo. The following formula was applied:

$$\Delta E_X = \Delta E'_X - \Delta E_{X,\text{Solv } A} - \Delta E_{X,\text{Solv } B}$$

where $\Delta E'_X$ was the quantity obtained with respect to the fragments in vacuo and $\Delta E_{X,\text{Solv } A}$ was the corresponding solvation energy of fragment A or fragment B with $\Delta E_{X,\text{Solv } B}$. Thus, the corrected ΔE_{Orb} and ΔE_{Solv} could be calculated. The true electronic dissociation energy ($-D_e$) could, furthermore, be computed by adding the overall fragment interaction energy ΔE_{Int} (the sum of all preceding terms) to the fragment preparation energy ΔE_{Prep} ; that is, the energy required to distort the fragments from their equilibrium geometry to the geometry of the fragments in the transition state. The equilibrium geometry of all unrelaxed fragments, with the inclusion of solvation, therefore had to be calculated.

A data set collection of computational results is available in the ioChem-BD repository^[24] and can be accessed through the link: <https://doi.org/doi:10.19061/iochem-bd-1-54>.

Acknowledgments

The authors acknowledge the Spanish Ministerio de Economía y Competitividad (MINECO) through projects CTQ2014-52824-R and CTQ2017-88777-R MINECO/AEI/FEDER/EU, the Severo Ochoa Excellence Accreditation SEV-2013-0319 and the CERCA Programme of Generalitat de Catalunya for financial support. N. A. G. B. gratefully acknowledges Fundação para a Ciência e Tecnologia (grants PTDC/QEQ-QIN/3414/2014 and SFRH/BPD/110419/ 2015) for funding.

Keywords: Density functional calculations · Molybdenum · Nanoreactor · Keplerate · Polyoxometalates

- [1] M. T. Pope, *Heteropoly and Isopoly Oxometalates*, Springer Verlag, Berlin, **1983**.
- [2] a) M. T. Pope, A. Müller, *Angew. Chem. Int. Ed. Engl.* **1991**, *30*, 34–48; *Angew. Chem.* **1991**, *103*, 56; b) A. Müller, M. T. Pope, *Polyoxometalates: From Platonic Solids to Anti-Retroviral Activity*, Springer, Dordrecht **1994**; c) A. Müller, F. Peters, M. T. Pope, D. Gatteschi, *Chem. Rev.* **1998**, *98*, 239–272; d) J. T. Rhule, C. L. Hill, D. A. Judd, R. F. Schinazi, *Chem. Rev.* **1998**, *98*, 327–358.
- [3] a) C. L. Hill, C. M. Prossermccartha, *Coord. Chem. Rev.* **1995**, *143*, 407–455; b) B. S. Jaynes, C. L. Hill, *J. Am. Chem. Soc.* **1995**, *117*, 4704–4705.
- [4] a) A. Müller, E. Krickemeyer, H. Bögge, M. Schmidtmann, F. Peters, *Angew. Chem. Int. Ed.* **1998**, *37*, 3360–3363; *Angew. Chem.* **1998**, *110*, 3567–3571; b) C. Schäffer, A. Merca, H. Bögge, A. M. Todea, M. L. Kistler, T. Liu, R. Thouvenot, P. Gouzerh, A. Müller, *Angew. Chem. Int. Ed.* **2009**, *48*, 149–153; *Angew. Chem.* **2009**, *121*, 155; c) U. Kortz, A. Müller, J. van Slageren, J. Schnack, N. S. Dalal, M. Dressel, *Coord. Chem. Rev.* **2009**, *253*, 2315–2327.
- [5] A. Ziv, A. Grego, S. Kopilevich, L. Zeiri, P. Miro, C. Bo, A. Müller, I. A. Weinstock, *J. Am. Chem. Soc.* **2009**, *131*, 6380–6382.
- [6] C. Bo, P. Miro, *Dalton Trans.* **2012**, *41*, 9984–9988.
- [7] S. Kopilevich, A. Gil, M. Garcia-Ratés, J. Bonet-Avalos, C. Bo, A. Müller, I. A. Weinstock, *J. Am. Chem. Soc.* **2012**, *134*, 13082–13088.
- [8] a) A. Rezaeifard, R. Haddad, M. Jafarpour, M. Hakimi, *J. Am. Chem. Soc.* **2013**, *135*, 10036–10039; b) S. Kopilevich, A. Müller, I. A. Weinstock, *J. Am. Chem. Soc.* **2015**, *137*, 12740–12743; c) S.-S. Wang, G.-Y. Yang, *Chem. Rev.* **2015**, *115*, 4893–4962.
- [9] C. Besson, S. Schmitz, K. M. Capella, S. Kopilevich, I. A. Weinstock, P. Kögerler, *Dalton Trans.* **2012**, *41*, 9852–9854.
- [10] R. Huisgen, *Angew. Chem. Int. Ed.* **1963**, *2*, 565–598; *Angew. Chem.* **1963**, *75*, 604–637.
- [11] N. A. G. Bandeira, S. Garai, A. Müller, C. Bo, *Chem. Commun.* **2015**, *51*, 15596–15599.
- [12] a) R. B. Woodward, R. Hoffmann, *J. Am. Chem. Soc.* **1965**, *87*, 395–397; b) R. B. Woodward, R. Hoffmann, *J. Am. Chem. Soc.* **1965**, *87*, 2511–2513; c) T. A. Albright, J. K. Burdett, M. H. Whangbo, *Orbital Interactions in Chemistry*, Wiley, Hoboken, **2013**.
- [13] R. G. Pearson, *Chemical Hardness: Applications from Molecules to Solids*, Wiley-VCH, Weinheim, **1997**.
- [14] E. J. Baerends, J. Autschbach, A. Bérces, C. Bo, P. M. Boerrigter, L. Cavallo, D. P. Chong, L. Deng, R. M. Dickson, D. E. Ellis, M. van Faassen, L. Fan, T. H. Fischer, C. F. Guerra, S. J. A. van Gisbergen, J. A. Groeneveld, O. V. Gritsenko, M. Grüning, F. E. Harris, P. v. d. Hoek, H. Jacobsen, L. Jensen, G. van Kessel, F. Kootstra, E. van Lenthe, D. A. McCormack, A. Michalak, V. P. Osinga, S. Patchkovskii, P. H. T. Philipsen, D. Post, C. C. Pye, W. Ravenek, P. Ros, P. R. T. Schipper, G. Schreckenbach, J. G. Snijders, M. Sola, M. Swart, D. Swerhone, G. te Velde, P. Vernooijs, L. Versluis, O. Visser, F. Wang, E. van Wezenbeek, G. Wiesenekker, S. K. Wolff, T. K. Woo, A. L. Yakovlev,

- T. Ziegler, *Scientific Computing and Modelling* ADF-2013.01, **2013**; <http://www.scm.com>.
- [15] A. D. Becke, *Phys. Rev. A: At. Mol. Opt. Phys.* **1988**, *38*, 3098–3100.
- [16] a) J. P. Perdew, *Phys. Rev. B: Condens. Matter Mater. Phys.* **1986**, *33*, 8822–8824; b) J. P. Perdew, *Phys. Rev. B: Condens. Matter Mater. Phys.* **1986**, *34*, 7406.
- [17] a) E. van Lenthe, E. J. Baerends, J. G. Snijders, *J. Chem. Phys.* **1993**, *99*, 4597–4610; b) E. van Lenthe, A. E. Ehlers, E. J. Baerends, *J. Chem. Phys.* **1999**, *110*, 8943–8953.
- [18] E. Van Lenthe, E. J. Baerends, *J. Comput. Chem.* **2003**, *24*, 1142–1156.
- [19] A. D. Becke, *J. Chem. Phys.* **1988**, *88*, 2547–2553.
- [20] A. Klamt, G. Schüürmann, *J. Chem. Soc. Perkin Trans. 2* **1993**, 799–805.
- [21] a) T. Ziegler, A. Rauk, *Theor. Chim. Acta* **1977**, *46*, 1–10; b) T. Ziegler, A. Rauk, *Inorg. Chem.* **1979**, *18*, 1755–1759.
- [22] K. Morokuma, *J. Chem. Phys.* **1971**, *55*, 1236–1244.
- [23] a) F. M. Bickelhaupt, E. J. Baerends in *Kohn–Sham Density Functional Theory: Predicting and Understanding Chemistry, Vol. 15* (Eds.: D. B. Boyd, K. B. Lipkowitz), Wiley VCH, New York, **2000**, pp. 1–86; b) M. v. Hopffgarten, G. Frenking, *WIREs Comput. Mol. Sci.* **2012**, *2*, 43–62.
- [24] M. Álvarez-Moreno, C. de Graaf, N. López, F. Maseras, J. M. Poblet, C. Bo, *J. Chem. Inf. Model.* **2015**, *55*, 95–103.

Received: February 1, 2018